Wang, H. Y., Göttlicher, J., Byrne, J. M., Guo, H. M., Benning, L. G., Norra, S. (2021): Vertical redox zones of Fe–S–As coupled mineralogy in the sediments of Hetao Basin – Constraints for groundwater As contamination. - Journal of Hazardous Materials, 408, 124924.

https://doi.org/10.1016/j.jhazmat.2020.124924

Vertical Redox Zones of Fe-S-As Coupled Mineralogy in the Sediments of Hetao Basin – Constraints for Groundwater As Contamination

H.Y. Wang[a*], J. Göttlicher[b], J.M. Byrne[c,d], H.M Guo[e], L. G. Benning[f,g], S. Norra[a]

[a]Institute of Applied Geoscience, Working Group of Environmental Mineralogy and Environmental System Analysis, Karlsruhe Institute of Technology (KIT), 76131 Karlsruhe, Germany

[b]Institute of Photon Science and Synchrotron Radiation, Karlsruhe Institute of Technology (KIT), 76344 Eggenstein-Leopoldshafen, Germany

[c]Geomicrobiology, Center for Applied Geosciences, University of Tübingen, 72074 Tübingen, Germany

[d]Now: School of Earth Sciences, University of Bristol, Wills Memorial Building, Queens Road, Bristol BS8 1RJ, United Kingdom

[e]State Key Laboratory of Biogeology and Environmental Geology, China University of Geoscience, 100083 Beijing, China

[f]GFZ German Research Center for Geoscience, 14473 Potsdam, Germany

[g]Department of Earth Sciences, Freie Universität Berlin, 12249 Berlin, Germany

Corresponding author*: hongyan.wang@kit.edu; +49017657764900

Abstract

The formation of iron-sulfur-arsenic (Fe-S-As) minerals during biogeochemical processes in As contaminated aquifers remains poorly understood despite their importance to understanding As release and transport in such systems. In this study, X-ray absorption and Mössbauer spectroscopies complemented by electron microscopy, and chemical extractions were used to examine vertical changes of As, Fe and S speciation for the example of sediments in the Hetao Basin.

Reduction of Fe(III), As(V) and SO_4^{2-} species were shown to co-occur in the aquifers. Iron oxides were observed to be predominantly goethite and hematite (36 – 12%) and appeared to decrease in abundance with depth. Furthermore, reduced As (including arsenite and As sulfides) and sulfur species (including S(-II), S(-I) and S^0) increased from 16% to 76% and from 13% to 44%, respectively.

Iron oxides were the major As carrier in the sediments, and the lower groundwater As concentration consists with less desorbable and reducible As in the sediments. The formation of As-Fe sulfides (e.g., As containing pyrite and greigite) induced by redox heterogeneities likely contribute to localized lower groundwater As concentrations. These results help to further elucidate the complex relationship between biogeochemical processes and minerals formation in As contaminated aquifers.

Keywords: XAS; speciation; Fe(III) oxides; Fe sulfides; arsenic

1. Introduction

The contamination of geogenic groundwater with arsenic (As) (> 10 µg/L: the World Health Organization standard) is a major threat to human health worldwide [1,2]. Large-scale exposure to high As groundwater mainly occurs in the river deltas of South and Southeast Asia including the Ganges-Brahmaputra-Meghna (GBM), the Red River and the Mekong River as well as inland basins draining the Yellow River and the Yangtze River [1],[3],[4],[5].

It is widely accepted that *in-situ* desorption of As from As-bearing Fe(III) oxides (including iron oxides, hydroxides, and oxyhydroxides) can lead to the release of As into groundwater [6–9]. Arsenic speciation and Fe mineralogy are important factors in this process, influencing As partition and therefore release into groundwater under stable geochemical conditions. Under reducing conditions, As(V) species are reduced to As (III) species which bond less strongly to Fe(III) oxides at circumneutral pH condition. Consequently, desorption is susceptible to shifting geochemical conditions such as groundwater flushing resulting from groundwater flow [10]. Furthermore, the Fe-bearing phases in sediments have different reactivities and therefore show different adsorption properties towards As. For example, poorly crystalline Fe(III) oxides provide much more adsorption sites for As than crystalline Fe(III) oxides and are much more likely to undergo abiotic and biotic reduction [11]. Characterizing the speciation and abundance of Fe(III) oxides and As in the sediments is therefore helpful for understanding the potential for As release into the groundwater.

Upon reduction of Fe(III) oxides, the formation of secondary Fe(II)-containing minerals can also influence the partitioning of As between sediments and groundwater [7],[12,13]. With large surface to volume ratios, Fe(II)-bearing minerals such as Fe sulfides (pyrite, FeS_2 or greigite, Fe_3S_4), Fe-carbonates (siderite, $FeCO_3$), Fe-phosphates (vivianite, $Fe_3(PO_4)_2.8H_2O$), or Fe oxides

(e.g., magnetite, Fe_3O_4) are each also able to sorb As to varying degrees, and can therefore retard As mobilization in groundwater [14–17]. For example, magnetite has been reported as the main secondary oxide and As carrier in Bangladesh sediments [18]. The formation of secondary Fe(II)-bearing minerals largely depends on the redox conditions in subsurface sediments and these influence the fate of heavy metals and metalloids [19–21]. It is necessary to develop a holistic understanding of the differences in Fe solid phases between redox zones to better understand heterogenous groundwater As contamination.

Recently, the influence of biogeochemical Fe-S-As cycling for As release and speciation in subsurfaces settings have been increasingly studied [22–24],[19]. The reduction of SO_4^{2-} and Fe(III) oxides can simultaneously occur at redox interfaces especially at neutral or slightly alkaline groundwater pH conditions [25]. On the one hand, saturation of Fe(II) and H_2S cause precipitation of Fe sulfides such as mackinawite (nominally FeS), pyrite (FeS_2), which can incorporate or adsorb As [26],[15],[27]. Furthermore, extra sulfide/S^0 may reduce poorly crystalline iron(III) oxides or produce As thiolations in porewaters, further increasing As mobilization potential in groundwater [28,29]. To date, the majority of published studies on sediments collected from the flood deltas/basins from South and Southeast of Asia focused on the relationship between Fe mineralogy and As speciation. These high-As containing groundwater typically have extreme low or undetectable SO_4^{2-} concentrations. In contrast As contaminated groundwaters in inland basins, especially those with arid/semi-arid climate e.g. Hetao Basin, have high SO_4^{2-} concentrations [4]. Such inland basins therefore represent the most suitable location to develop understanding of the interplay between Fe-S-As redox reactions and groundwater As concentration.

The Hetao Basin in North China is a typical alluvial-lacustrine inland basin draining the Yellow River. Groundwater As concentrations vary between < 1 µg/L and 900 µg/L, with 70% of analyzed

groundwater samples being higher than 10 µg/L [30]. Groundwater SO_4^{2-} concentration is up to 3000 mg/L with median values around 90 mg/L [29]. Previous isotopic and hydro-chemical studies showed that As mobilization was closely linked to the reduction of Fe(III) oxides and SO_4^{2-} [9],[29],[31]. However, there is so far no detailed mineralogical evidence about Fe-S-As coupled reactions in the sediments. In this study, we analyzed sediments from the Hetao Basin with a range of geochemical based techniques with spectroscopic (XAS, ^{57}Fe Mössbauer) and electron microscopic techniques to (1) identify different redox zones along a sediment core depth profile (2) examine vertical changes in the coupling between mineral phases and As, Fe and S speciation, and (3) understand the influence of Fe-S-As coupled minerals on groundwater As concentrations.

2. Material and Methods

2.1 Field area

The Hetao Basin, covering an area of 13,000 km^2, is one of the typical alluvial-lacustrine Quaternary inland basins in northern China within the Yellow River catchment area. Groundwater is mainly extracted from depths < 100 m for irrigation usage, with family-based drinking water mainly obtained from depths of 20 to 30 m. Groundwater tables are vulnerable to irrigations, and have been shown to drop as a result of extraction (from mid-April to early September) [32]. The study area (Shahai) is located in the flat plain of the Hetao Basin, and it is one of the areas' most seriously affected by groundwater As contamination. Further information about the study area is detailed in [32,33].

2.2 Well installation, sediments sampling and groundwater sampling

A multi-level well (K1) was drilled by CUGB (China University of Geoscience, Beijing) in October 2015 using a circulatory drilling method. After the core sections were brought to the

surface, sediments were cut into 10 cm segments and immediately wrapped with tinfoil, and sealed in N_2-purged bags. Subsamples (5 cm segments) were transported to Karlsruhe Institute of Technology (KIT) and stored at -80 ℃. The physical parameters and chemical compositions of the groundwater were monitored from April to November 2016 (six times during the non-irrigation season and eleven times during irrigation season) by members of China University of Geosciences (Beijing) (CUGB). Further details about sediment sampling, and groundwater monitoring as well as water samples analyses are detailed in [32,33].

2.3 Bulk sediment characterization

Part of each sample was freeze-dried and ground into a powder. The basic characterization of the sediments described in Wang et al.[33] was complemented in the current study with detailed analyses. For this, iron content in the sediments was analyzed by wavelength dispersive X-ray spectrometry (WDX, S4 Explorer, Bruker AXS) with measurement accuracy (within ±5%) being regularly controlled with a standard material (AGV-1, USGS). Total sulfur (TS) and organic carbon (TOC) content were measured by carbon-sulfur-analyzer (CS-2000, Leybold Heraeus, Germany) with TOC obtained after removing inorganic carbon by repeated addition of 20% HCl (Superpure, Merke). The measurement accuracy and precision (100 ± 2%) was regularly checked with a steel standard 92400-3050 (Eltra). Arsenic contents in the sediments was determined by digestion prior to measurement by Hydride Generation Flow Injection Atomic Absorption Spectroscopy (HG-FIAS). The details about acid digestion method is provided in **Supplementary text 1**. The recovery (100 ± 5%) was regularly checked by including standards GXR-5 and RGM-1 into the digestion workflow. The detection limit of the HG-FIAS analyses was 0.1 μg/L.

2.4 Sequential extractions for As and 2M HCl extractions

A five-step sequential extraction was used to analyze As partitioning in the sediments. The extraction procedure is shown in **Table S1** and is based on Keon et al. [34] and Poulton and Canfield [35]: (1) "ligand-displaceable" (1.0 M $H_2PO_4^-$, pH = 5.0, S1), (2) "AVS (acid volatile sulfides), carbonates-precipitated" (1.0 M $CHCOO^-$, pH = 4.5, S2), (3) "amorphous Fe oxides and magnetite-precipitated" (0.17 M oxalic acid, pH = 3.0, S3), (4) "crystalline Fe oxides-precipitated" (citrate-bicarbonate-dithionite (CBD), S4), and (5) "Fe(II) sulfides-precipitated nominally from dissolution of pyrite" (12 M HNO_3, S5). For the extraction, 0.5 g of fresh sediments was weighed into centrifuge tubes and shaken at 300 rpm followed by addition of an appropriate amount of deoxygenated chemical solution. After each extraction step, solutions were filtered using 0.45 µm cellulose acetate filters (Whatman) followed by centrifugation at 4500 rpm for 15 min. Resulting, samples were washed once using 50 mL ultrapure water. Arsenic and Fe concentrations were measured by inductively coupled plasma mass spectrometry (ICP-MS, X-Series, Thermo Fisher), and the resulting extracted As from each step was converted into As content in the dried bulk sediments.

In a second extraction mode, we used HCl extraction with fresh sediments to obtain the reactive Fe phases [36]. For this extraction, around 2 g sediments were weighed into centrifuge tubes, mixed with 15 mL 2 M HCl (Superpure, Merck) and shaken. After 20 h, the solutions were filtered through 0.45 µm cellulose acetate filters (Whatman). Total Fe concentration was measured by inductively coupled plasma-optical emission spectrometry (ICP-OES, Spectro CirosCCD, Kleve, Germany). The Fe(II) concentration in the resulting extracts was measured by photometry at 562 nm using the ferrozine method [37].

2.5 Electron microscopy

151 Parts of the sediment samples were separated from intact cores and embedded in an As free-resin
152 (Araldite, 2020) and dried in a glovebox (Jacomex, 100% Ar). Sections of 1-mm thickness were
153 cut and polished down to a thickness of 80 μm. Thin sections were stored in the glovebox until
154 analysis. Carbon-coated thin sections were imaged and spectrally analyzed at the GFZ Research
155 Center for Geosciences in Potsdam, Germany, using field emission scanning electron microscope
156 (FE-SEM, Zeiss Ultra Plus) equipped with an energy dispersive X-ray (EDX) detector for
157 qualitative elemental analyses. Images were acquired at an acceleration voltage of 3 kV using a 10
158 mm aperture distance using an In-lens secondary electron detector.

159 **2.6 ^{57}Fe Mössbauer spectroscopy**

160 Selected sediments were analyzed using ^{57}Fe Mössbauer spectroscopy at the University of
161 Tübingen, Germany. Approximately 100 mg sediments were separated from each intact core for
162 analysis. Inside a glovebox (100% N_2 atmosphere), dried sample powders were loaded into
163 Plexiglas holders (area 1 cm^2), forming a thin disc. Samples were kept in airtight jars under anoxic
164 conditions at -20 °C until measurement. Holders were inserted into a closed-cycle exchange gas
165 cryostat (Janis cryogenics) under a backflow of He to minimize exposure to air. Spectra were
166 collected at 20 K using a constant acceleration drive system (WissEL) in transmission mode with
167 a ^{57}Co/Rh source. All spectra were calibrated against a 7 μm thick α-^{57}Fe foil that was measured
168 at room temperature. The analysis was carried out using Recoil (University of Ottawa) and the
169 Voigt Based Fitting (VBF) routine [38], with the half width at half maximum (HWHM)
170 constrained to 0.13 mm/s during fitting.

171 **2.7 Bulk X-ray absorption spectroscopy**

The speciation of As, S and Fe in selected sediment samples were measured using X-ray absorption spectroscopy (XAS) analysis at the SUL-X beamline at the synchrotron radiation facility of the KIT. Samples were ground into powder after drying in a glovebox (Jacomex, 100% Ar) with O_2 level less than 1 ppm). A sample mass for Fe K-edge XAS analysis, calculated by the program XAFSmass, was mixed with boron nitride (Sigma-Aldrich) before analysis. For As and Fe K-edge XAS analysis, powdered samples were suspended in deoxygenated water in the glovebox, drop-casted onto Kapton tape, and sealed using a second piece of Kapton tape. For S K-edge XAS measurements, dried samples were directly loaded onto the Kapton tape surface. Prepared samples were stored in the N_2-filled bags to protect from O_2 before transferring into the measurement chamber. Samples are analyzed under ultra-vacuum conditions in the beam chamber. At least three scans were collected per sample for each As, Fe and S K-edge XAS spectrum. During the data collection, line shapes and peak positions were monitored, with no difference between scans for each sample, indicating no redox change during analyses. Data reduction and analysis of the XAS spectra were performed using the Athena software package [39]. Experimental and data analysis procedures are outlined in the **supplementary text 2**. Besides the samples analyses here, we also compared our data with XAS spectra and Mössbauer spectra for sample from another depth (80.5 m) that had been previously analyzed [33].

3. Results

3.1 Vertical profile of groundwater chemical compositions and As concentration

Groundwater monitoring data in the well are detailed in Zhang et al. [32]. The data shows that in the shallow zone SO_4^{2-} concentrations increased from 400 mg/L to 1000 mg/L from 15 - 16 m to 27 - 28 m, but that it stabilized at around 200 mg/L in the deeper zone. Arsenic concentration also generally decreased with depths. Specifically, it increased from 90 µg/L at depth of 15 - 16 m to

120 µg/L at depth of 20 - 21 m and slightly decreased to 90 µg/L at depth of 27 - 28 m in the shallow zone, while it was less than 50 µg/L in the deep zone (**Fig. 1)**.

3.2 Sediments profile characterization

A ~ 2 m thick clay layer located at a depth of 39.5 m separated the shallow and deep groundwater zone. Aquifer sediments were mainly composed of fine sand and silt, and the color varied from gray to dark gray. In general, sediments from the deep zone had a darker color than the shallow zone. A thin peat layer was identified at a depth of around 80 m with dark color (**Fig. 1**). Lithology profile of the borehole presents general sedimentation textures in the Hetao Basin [29],[40].

Total organic carbon (TOC) contents ranged from 0.04% to 0.59% with lower TOC contents in the aquifer sediments (~0.05%). Surface sediments had higher S content (~ 1000 mg/kg) than aquifer sediments (average 285 mg/kg). Iron content in the sediments ranged from ~1 % to ~ 6% with lower Fe content shown in silt/sand. Sediments had As contents ranging from 5 mg/kg to 46 mg/kg, while primary aquifer sand/silt contained 5 mg/kg to 9 mg/kg (**Fig. 2**). Highest As contents were found in sediment samples from ~29 m (38 mg/kg) and 80 m (46 mg/kg).

3.3 Sediments mineralogy and iron speciation

Predominant minerals in the sediments included quartz, feldspars, mica and clay minerals [41]. Additional clastic trace minerals including hornblende, augite and ilmenite were qualitatively identified by SEM-EDX analysis (data not shown). Iron oxides which might have different morphologies were identified **(Fig. 3a, b and c)**. In most cases, the Fe oxides were surrounded by or coated on the surface of clay minerals. In addition, Fe sulfides nominally FeS_2, pyrite as shown in the EDX spectra) were identified in samples from 29 m (**Fig. 3d**). A previous study identified the presence of greigite in the peats (at depth of 80 m) [33] (**Fig. 3e**).

Mössbauer spectroscopic analysis suggested that Fe was present in several phases including: Fe(II), silicate-bound Fe(III), or goethite/hematite (**Fig. 4a** and **Table S3**). The hyperfine parameters of the Fe(II) phase (isomer shift: 1.19-1.27 mm/s and quadrupole splitting: 2.34-2.85 mm/s) are potentially indicative of the phyllosilicates shown in the sediments. A narrow doublet (isomer shift: 0.41-0.48 mm/s, quadrupole splitting: 0.77-1.16 mm/s) was also required for an accurate fit which is indicative of ferric ions (Fe^{3+}) that could correspond to a phyllosilicates, though the presence of short range ordered phases (e.g. ferrihydrite) or low spin ferrous ion (Fe^{2+}) phases (e.g. pyrite) cannot be ruled out [42]. From the Liner combination fitting (LCF) of the Fe K-edge EXAFS spectra, it was revealed that goethite and hematite comprised 12% - 35% (mol %) of the Fe speciation in the sediments (**Fig. 4b and Table 1**). The difference between the Fe K-edge EXAFS fits and the Mössbauer fits in terms of Fe(III) oxides contents was less than 10 % and which is considered acceptable [43] (**Table 1 and Table S3**).

Iron sulfides were shown as mono FeS (mackinawite) in most aquifer sediments with primarily low content indicated by Fe K-edge EXAFS fitting (**Fig. 4b**). However, pyrite was not detected at the depth of 29 m as revealed by SEM-EDX, likely due to an abundance of pyrite is lower than the detection limit of Fe EXAFS fits, which has been estimated to be 5% by fitting a set of mixed standards with known fractions [44],[20].

The redox characteristics of Fe phases was deduced from the combined 2M HCl extractions and Fe K-edge XANES. The reactive Fe extracted by 2M HCl included poorly crystalline Fe(III) oxides, acid volatile sulfides (AVS), carbonates as well as part of Fe adsorbed or incorporated in the silicates [7],[45],[46]. This extractable Fe comprised 28% to 51% of total Fe in the sediments (**Table S5**), while the Fe(II) content ranged from 29% to 72% of total extractable Fe (except peat layer) (**Fig. 5a**). Noticeably, the Fe(II)/Fe ratio obtained from the 2M HCl extractions is not

comparable to the Mössbauer result, as Mössbauer results showed all Fe in the sediments instead of reactive Fe. Depth patterns of the leached Fe(II)/Fe_{total} showed increasing trend with depth (R^2 = 0.55, **Fig. 6a**), while it sharply increased from 30% to 50% at a depth of 7 m (**Fig. 5a**). In the Fe K-edge XANES spectra, a peak at an energy of ~7120 keV suggests the presence of Fe(II) phases [44],[47], the intensity of these generally increased with depth, consistent with the results from the 2M HCl extractions. Furthermore, Fe K-edge EXAFS showed that the proportion of Fe(III) oxides decreased with depth (R^2 = 0.94) (**Fig. 6b**), comprising of 35 mol % of the Fe species in the top sediments (~ 7 m), decreasing to 27 - 28% in the shallow zone and further decreasing to 22% - 12% in the deep zone. Unfortunately, Mössbauer result cannot be used to indicate the redox profile, when only few samples were analyzed.

3.4 Arsenic extractability

Desorbable (ligand-reducible) As (1.0 – 11 mg/kg) accounted for 23% - 56% of the total extractable As in the sediments, while reducible As (sum of ammonium oxalate and CBD extractable) (2.0 – 10.4 mg/kg) accounted for 32% - 65% of total extractable As (**Table 2**). Only a limited amount of As was extracted by $CHCOO^-$ (< 1.2 mg/kg) and HNO_3 (< 1.4 mg/kg) (except for peat layers). The contents of desorbable and reducible As were positively correlated to Fe(III) oxides (R^2 = 0.89, **Fig. 6c**), showing a decreasing trend with depth. Noticeably, the extractable As content at a depth of 29 m was much lower than 38 mg/kg, and no pyrite-associated As could be extracted by HNO_3, which further suggests that pyrite was low in abundance and heterogeneously distributed in the sediments.

3.5 Arsenic and sulfur speciation

The LCF of the As K-edge XANES spectra (**Fig. 5c and Table 1**) revealed that arsenate comprised 28% to 84% of the total As in the primary sediments, but that its abundance sharply declined from 84% at a depth of 4 m to 54% at a depth of 6 m, and further decreasing with depth (R^2 = 0.59, **Fig. 6d**). Conversely, the arsenite content increased with depth. At a depth of 29 m, 62% of As was present as As sulfides (arsenian pyrite/arsenopyrite), consistent with the pyrite found in the sediments. The As sulfides accounted for 41% of total As in the peat layer (**Fig. 5c and Table 1**). Finally, sulfur K-edge XANES LCF showed that S mainly existed as SO_4^{2-} (vary from 49% to 93%). Reduced sulfur (including S(-I) and S(-II)) and zero-valent sulfur (S^0) was detected at most depths except in the surface sediments at 4 m. The ratio of reduced sulfur was generally higher in the deep zone than the shallow zone (**Fig. 5d and Table 1**).

4 Discussion

4.1 Sediment profile redox zonation

The surface sediments were dominated by oxidized phases including sulfates, As(V) species and Fe(III)-containing solid phases, due to oxygen penetration into sediments pores. Reduction of As(V) species, Fe(III), and SO_4^{2-} is present near the groundwater table (6 - 7 m). The co-occurrence of reduction reactions were independent of the thermodynamic redox ladder, which suggested the electron accepting process followed the order of As(V) > Fe(III) > SO_4^{2-} [48,49]. These observations are consistent with previous suggestions that Fe(III) and SO_4^{2-} reduction co-occur in near neutral or slightly alkaline subsurface environments [25]. Underlying the aquitard (~ 40 m), SO_4^{2-} reduction generally increases with relatively higher ratio of reduced sulfur species, which is consistent with lower redox values in the groundwater of deep zone [32]. These results together indicate that redox zones in the alluvial-lacustrine sediments of the Hetao Basin are generally controlled by the physiographic properties, including the groundwater table and sediment depths.

284 In contrast, the aquifer redox conditions in the floodplain of South and Southeast Asia such as the
285 Red River Delta, the Mekong River Delta are controlled by depositional environments with
286 reducing conditions widely developed in the Holocene fluvial sediments, while the Pleistocene
287 aquifer are characterized by sub-oxic conditions [50–52].

288 Noticeably, redox heterogeneities exist in the sediments. Even though the reduced Fe, As and S
289 species generally increase with depth, some sediment lenses show pronounced peaks, related to
290 the redox heterogeneities in the sediments. For example, organic carbon-rich lenses including clay
291 and peat layers have more reduced As, Fe and S species in comparison with surrounding sediments.
292 High amounts of organic matter in those layers stimulates the *in-situ* reduction of As, Fe and S and
293 therefore Fe sulfide formation.

294 **4.2 Speciation and reactivity of Fe-S-As coupled minerals in the sediments profile**

295 Dominant Fe(III) oxides in the sediments of the Hetao Basin are goethite and hematite, similar to
296 sediments from the Red River Delta and the Mekong Delta [53],[12],[54,55]. In contrast to the
297 formation of secondary Fe(II) or Fe(II/III) solid phases such as siderite, vivianite, and magnetite
298 which is well-documented in the floodplains of South and Southeast of Asia, in the sediments of
299 the Hetao Basin [7],[56], only As containing Fe sulfides were detected. However, trace amounts
300 of Fe sulfides do not appear to be the major sink of Fe(II), which is a consequence of reductive
301 dissolution of the ample present Fe(III) oxides. This indicates that Fe(II) is most likely
302 adsorbed/substituted back into clay minerals which can provide a large surface for Fe adsorption
303 [57,58]. The relatively higher adsorption affinity for Fe(II) is probably due to slightly alkaline pH
304 conditions in the aquifers, in such adsorption of Fe(II) to clay minerals is favored at pH above 6.0
305 [59]. This concept explains the lower average Fe concentration in the alluvial-lacustrine

306 groundwater in the Yellow River catchment as well as decoupling of Fe and As concentration in
307 the groundwater under reducing conditions [60],[61].

308 Natural Fe(III) oxides are impure and are typically highly variable in crystallinity, incorporation
309 or substitution of other elements in their structure is common, thus making predictions of their
310 reactivities challenging [56]. We used, a combination of quantification methods for our Fe(III)
311 oxides and combined with Fe EXAFS LCF and As reactivities by sequential extractions. This
312 enabled us to better understand of the As partition to Fe(III) oxides in the sediments. Correlations
313 between Fe(III) oxides and desorbable and reducible As suggests that Fe(III) oxides are the main
314 As carrier in the sediments. These findings corroborates with previous studies that the adsorption
315 sites for As are limited and linked to the amount of Fe(III) oxides in aquifer sediments [13],[62].
316 The adsorption coefficient of As to Fe(III) oxides in the sediments of Hetao Basin is around $0.9 \times$
317 10^{-3}, based on the assumption that desorbable and reducible As are totally carried by Fe(III) oxides.
318 A similar partition coefficient of As in Fe(III) oxides was documented for the Red River floodplain
319 by Postma et al. [13]. The calculated adsorption capabilities of Fe(III) oxides for As provide the
320 fundamental knowledge for modeling As mobilization in the groundwater especially in the
321 alluvial-lacustrine aquifers draining the Yellow River and the Yangtze River.

322 Detection of mono Fe sulfides (mackinawite) in the primary sediments is consistent with the dark
323 gray color found in the aquifer sediments, which is caused by Fe sulfides coating the sand particles
324 [63]. Arsenic can form poorly crystalline arsenic sulfides that could adsorb to mackinawite [64].
325 However, the adsorption efficiency of mackinawite for As is limited as indicated by As XANES
326 analysis. This could be linked to the formation and stability of FeS in the groundwaters [65]. The
327 further transformation of FeS to pyritie or greigite is a more likely process that provides the
328 adsorption/incorporation sites and stable sinks for As. This was identified by the higher As content

in the corresponding sediments than near-by layers and the existence of large proportions of As sulfides.

4.3 Significance of Fe-S-As coupled mineralization for geogenic groundwater As contamination

Redox cycling of Fe minerals in the redox front influences the partition of As. In the Hetao Basin, the groundwater table decreases during the irrigation season, allowing penetration of O_2 to cause the temporary formation of Fe(III) oxides by oxidation of Fe(II), therefore providing adsorption surfaces for dissolved As. Conversely, raising of the groundwater table and ensuing anoxic conditions will causes As release into groundwater via Fe(III) oxide reduction. Underlying the redox front, stable Fe and As reduction occurs simultaneously. Generally higher groundwater As concentrations are present in the shallow zone and less in the deep zone, even though the deep zone is more reducing. This can be due to lower abundance of Fe(III) oxides and desorbable and reducible As in the deep zone. The lower As concentration in the groundwater with less solid phase desorbable As and reducible As in the corresponding sediments intervals (R^2 = 0.65) **(Fig. 7)** further provides solid evidence that *in-situ* desorption of As from Fe(III) oxides causes groundwater As contamination. The decrease of Fe(III) oxide abundance and corresponding desorb-able/reducible As with depth can be related to the longer sediments reduction and flushing history. Sediments from deeper depths have longer exposure to reducing conditions than overlying sediments, corresponding to the accumulation of reduced phases (Fe(II), As(III)) and partial release of out of the system.

Redox heterogeneities in the sediment profile hinders the effort to estimate the redox reactions in the aquifer and thereby model groundwater As concentration. For example, localized formation of greigite and pyrite can very well provide a stable sink for As. Furthermore, S^0 detected in the

sediments especially in the clay samples could lead to thiolation via the reaction between H_2S/S^0 and As species in the reduced sulfidic aquifer, which in turn can promote further As mobilization [24],[66,67], Whether thioarsenate species exist in the groundwater and to what degree influences As mobility may also be related to the ratio of Fe, S and As in the sediments, which needs further investigation.

5. Conclusions

In this study, we have defined the redox profile of Fe-S-As in an alluvial-lacustrine inland Hetao basin. The sediment redox profile is generally controlled by physiographic features (e.g. groundwater table and sediment depths). Underlying the groundwater table, reduction of SO_4^{2-}, Fe and As co-occurs, while SO_4^{2-} reduction ratio is generally higher in the deep zone. Iron oxides seem to be the major carrier of As. The As mobilizes into groundwater mainly via *in-situ* desorption from Fe(III) oxides (goethite and hematite). The abundance of desorbable and reducible As content exhibited a decreasing trend with depth, which is most probably due to longer flushing history, during which part of As is flushed out of the system followed by reductive release into the groundwater. Iron sulfides are the main secondary minerals formed in the aquifer following changing redox and Fe(II) production. Among them, mackinawite was evidenced as having a limited adsorption/incorporating ability for As, while greigite and pyrite provide a more stable sink for As under reducing conditions. The heterogenous distribution and low contents of Fe sulfides formed in sediment lenses might contribute to the lower groundwater As concentrations under reducing conditions. The influences of such small-scale redox heterogeneity and their role for large-scale groundwater As pollution need further research.

Conflicts of interest

The authors declare no conflict of interest

Acknowledgments

The Authors are thankful for the technical assistance from Claudia Moessner (ICP-MS), Beate Oetzel (CSA), Sathish Mayanna (SEM-EDX). We Thank Ralf Steininger, Andrew Thomas for his support during collection of Fe, As and S K-edge XAS data at ANKA. The authors also acknowledge other members from CUGB group for their assistance during field trip to Hetao Basin and travel funding from GRACE graduate program at KIT. We are grateful for the constructive suggestios from three reviewers. The author Hongyan Wang is supported by Chinese scholarship Council Grant No. 201606400055.

Authors contribution

H. Y. Wang: investigation, writing–original draft, funding acquisition; J. Göttlicher: investigation, writing-review & editing; J. M. Byrne: investigation, writing–review & editing; H. M. Guo: writing–review & editing, funding acquisition; L. G. Benning: investigation, writting-review & editting; S. Norra: writing–review & editing, supervision, funding acquisition. The study is based on the Sino-German cooperation initiated by H. Guo and S. Norra and was inspired by their ideas.

References

[1] S. Fendorf, H.A. Michael, A. van Geen, Spatial and Temporal Variations of Groundwater Arsenic in South and Southeast Asia, Science. 328 (2010) 1123–1127. https://doi.org/10.1126/science.1172974.

[2] J. Podgorski, M. Berg, Global threat of arsenic in groundwater, Science. 850 (2020) 1–31.

[3] D.K. Nordstrom, Worldwide Occurrences of Arsenic in Ground Water, Science. 296 (2002) 64–65. https://doi.org/10.1007/b101867.

[4] Y. Wang, K. Pi, S. Fendorf, Y. Deng, X. Xie, Sedimentogenesis and hydrobiogeochemistry of high arsenic Late Pleistocene-Holocene aquifer systems, Earth-Science Rev. (2017) 0–1. https://doi.org/10.1016/j.earscirev.2017.10.007.

[5] H. Guo, D. Wen, Z. Liu, Y. Jia, Q. Guo, A review of high arsenic groundwater in Mainland and Taiwan, China: Distribution, characteristics and geochemical processes, Appl. Geochemistry. 41 (2014) 196–217. https://doi.org/10.1016/j.apgeochem.2013.12.016.

[6] F.S. Islam, A.G. Gault, C. Boothman, D. a Polya, J.M. Charnock, D. Chatterjee, J.R. Lloyd, Role of metal-reducing bacteria in arsenic release from Bengal delta sediments., Nature. 430 (2004) 68–71. https://doi.org/10.1038/nature02638.

[7] A. Horneman, A. van Geen, D. V. Kent, P.E. Mathe, Y. Zheng, R.K. Dhar, S. O'Connell, M.A. Hoque, Z. Aziz, M. Shamsudduha, A.A. Seddique, K.M. Ahmed, Decoupling of As and Fe release to Bangladesh groundwater under reducing conditions. Part I: Evidence from sediment profiles, Geochim. Cosmochim. Acta. 68 (2004) 3459–3473.

https://doi.org/10.1016/j.gca.2004.01.026.

[8] J.M. McArthur, P. Ravenscroft, S. Safiulla, M.F. Thirlwall, Arsenic in groundwater: Testing pollution mechanisms for sedimentary aquifers in Bangladesh, Water Resour. Res. 37 (2001) 109–117. https://doi.org/10.1029/2000WR900270.

[9] H. Guo, C. Liu, H. Lu, R.B. Wanty, J. Wang, Y. Zhou, Pathways of coupled arsenic and iron cycling in high arsenic groundwater of the Hetao basin, Inner Mongolia, China: An iron isotope approach, Geochim. Cosmochim. Acta. 112 (2013) 130–145. https://doi.org/10.1016/j.gca.2013.02.031.

[10] K.G. Stollenwerk, G.N. Breit, A.H. Welch, J.C. Yount, J.W. Whitney, A.L. Foster, M.N. Uddin, R.K. Majumder, N. Ahmed, Arsenic attenuation by oxidized aquifer sediments in Bangladesh, Sci. Total Environ. 379 (2007) 133–150. https://doi.org/10.1016/j.scitotenv.2006.11.029.

[11] O. Larsen, D. Postma, R. Jakobsen, The reactivity of iron oxides towards reductive dissolution with ascorbic acid in a shallow sandy aquifer (Rømø, Denmark), Geochim. Cosmochim. Acta. 70 (2006) 4827–4835. https://doi.org/10.1016/j.gca.2006.03.027.

[12] D. Postma, F. Larsen, N.T. Minh Hue, M.T. Duc, P.H. Viet, P.Q. Nhan, S. Jessen, Arsenic in groundwater of the Red River floodplain, Vietnam: Controlling geochemical processes and reactive transport modeling, Geochim. Cosmochim. Acta. 71 (2007) 5054–5071. https://doi.org/10.1016/j.gca.2007.08.020.

[13] D. Postma, T.K.T. Pham, H.U. Sø, V.H. Hoang, M.L. Vi, T.T. Nguyen, F. Larsen, H.V. Pham, R. Jakobsen, A model for the evolution in water chemistry of an arsenic contaminated aquifer over the last 6000 years, Red River floodplain, Vietnam, Geochim.

Cosmochim. Acta. 195 (2016) 277–292. https://doi.org/10.1016/j.gca.2016.09.014.

[14] Y. Wang, P. Le Pape, G. Morin, M. Asta, G. King, B. Bartova, E. Suvorova, M. Frutschi, M. Ikogou, V.H.C. Pham, P. Le Vo, F. Herman, L. Charlet, R. Bernier-Latmani, Arsenic speciation in Mekong Delta sediments depends on their depositional environment, Environ. Sci. Technol. (2018) acs.est.7b05177. https://doi.org/10.1021/acs.est.7b05177.

[15] B.D. Kocar, T. Borch, S. Fendorf, Arsenic repartitioning during biogenic sulfidization and transformation of ferrihydrite, Geochim. Cosmochim. Acta. 74 (2010) 980–994. https://doi.org/10.1016/j.gca.2009.10.023.

[16] J.P.H. Perez, H.M. Freeman, A.P. Brown, C.M. Van Genuchten, K. Dideriksen, M. S'Ari, D.J. Tobler, L.G. Benning, Direct Visualization of Arsenic Binding on Green Rust Sulfate, Environ. Sci. Technol. 54 (2020) 3297–3305. https://doi.org/10.1021/acs.est.9b07092.

[17] J.P.H. Perez, A.A. Schiefler, S.N. Rubio, M. Reischer, N.D. Overheu, L.G. Benning, D.J. Tobler, Arsenic removal from natural groundwater using "green rust": Solid phase stability and contaminant fate, J. Hazard. Mater. 401 (2021). https://doi.org/10.1016/j.jhazmat.2020.123327.

[18] M.L. Polizzotto, C.F. Harvey, G. Li, B. Badruzzman, A. Ali, M. Newville, S. Sutton, S. Fendorf, Solid-phases and desorption processes of arsenic within Bangladesh sediments, Chem. Geol. 228 (2006) 97–111. https://doi.org/10.1016/j.chemgeo.2005.11.026.

[19] J.J. Lemonte, J.W. Stuckey, J.Z. Sanchez, R. Tappero, J. Rinklebe, D.L. Sparks, Sea Level Rise Induced Arsenic Release from Historically Contaminated Coastal Soils, Environ. Sci. Technol. (2017). https://doi.org/10.1021/acs.est.6b06152.

[20] S.M. Shaheen, J. Rinklebe, T. Frohne, J.R. White, R.D. DeLaune, Redox effects on release kinetics of arsenic, cadmium, cobalt, and vanadium in Wax Lake Deltaic freshwater marsh soils, Chemosphere. 150 (2016) 740–748. https://doi.org/10.1016/j.chemosphere.2015.12.043.

[21] T. Frohne, J. Rinklebe, R.A. Diaz-Bone, G. Du Laing, Controlled variation of redox conditions in a floodplain soil: Impact on metal mobilization and biomethylation of arsenic and antimony, Geoderma. 160 (2011) 414–424. https://doi.org/10.1016/j.geoderma.2010.10.012.

[22] K. Pi, Y. Wang, D. Postma, T. Ma, C. Su, X. Xie, Vertical variability of arsenic concentrations under the control of iron-sulfur-arsenic interactions in reducing aquifer systems, J. Hydrol. 561 (2018) 200–210. https://doi.org/10.1016/j.jhydrol.2018.03.049.

[23] H.Y. Jeong, Y. Han, S.W. Park, K.F. Hayes, Aerobic oxidation of mackinawite (FeS) and its environmental implication for arsenic mobilization, Geochim. Cosmochim. Acta. 74 (2010) 3182–3198. https://doi.org/10.1016/j.gca.2010.03.012.

[24] N. Kumar, V. Noël, B. Planer-friedrich, J. Besold, J. Lezama, J.R. Bargar, G.E. Brown, S. Fendorf, K. Boye, Redox Heterogeneities Promote Thioarsenate Formation and Release into Groundwater, Environ. Sci. Technol. (2020). https://doi.org/10.1021/acs.est.9b06502.

[25] C.M. Bethke, R.A. Sanford, M.F. Kirk, Q. Jin, T.M. Flynn, The thermodynamic ladder in geomicrobiology, Am. J. Sci. 311 (2011) 183–210. https://doi.org/10.2475/03.2011.01.

[26] K. Pi, Y. Wang, X. Xie, T. Ma, C. Su, Y. Liu, Role of sulfur redox cycling on arsenic mobilization in aquifers of Datong Basin, northern China, Appl. Geochemistry. 77 (2017) 31–43. https://doi.org/10.1016/j.apgeochem.2016.05.019.

[27] M. Mihaljevic, Microbial sulfidogenesis of arsenic in naturally contaminated wetland soil, Geochim. Cosmochim. Acta. 267 (2019) 33–50. https://doi.org/10.1016/j.gca.2019.09.021.

[28] J. Sun, A.N. Quicksall, S.N. Chillrud, B.J. Mailloux, B.C. Bostick, Arsenic mobilization from sediments in microcosms under sulfate reduction, Chemosphere. 153 (2016) 254–261. https://doi.org/10.1016/j.chemosphere.2016.02.117.

[29] H. Guo, Y. Zhou, Y. Jia, X. Tang, X. Li, M. Shen, H. Lu, S. Han, C. Wei, S. Norra, F. Zhang, Sulfur Cycling-Related Biogeochemical Processes of Arsenic Mobilization in the Western Hetao Basin, China: Evidence from Multiple Isotope Approaches, Environ. Sci. Technol. (2016) acs.est.6b03460. https://doi.org/10.1021/acs.est.6b03460.

[30] H. Guo, S. Yang, X. Tang, Y. Li, Z. Shen, Groundwater geochemistry and its implications for arsenic mobilization in shallow aquifers of the Hetao Basin, Inner Mongolia, Sci. Total Environ. 393 (2008) 131–144. https://doi.org/10.1016/j.scitotenv.2007.12.025.

[31] Y. Jia, H. Guo, Y. Jiang, Y. Wu, Y. Zhou, Hydrogeochemical zonation and its implication for arsenic mobilization in deep groundwaters near alluvial fans in the Hetao Basin, Inner Mongolia, J. Hydrol. 518 (2014) 410–420. https://doi.org/10.1016/j.jhydrol.2014.02.004.

[32] Z. Zhang, H. Guo, S. Liu, H. Weng, S. Han, Z. Gao, Mechanisms of groundwater arsenic variations induced by extraction in the western Hetao Basin, Inner Mongolia, China, J. Hydrol. 583 (2020) 124599. https://doi.org/10.1016/j.jhydrol.2020.124599.

[33] H.Y. Wang, J.M. Byrne, J.P.H. Perez, A.N. Thomas, J. Goettlicher, H.E. Hofer, S. Mayanna, A. Kontny, A. Kappler, H.M. Guo, L.G. Benning, S. Norra, Arsenic sequestration in pyrite and greigite in the buried peat of As-contaminated aquifers,

Geochim. Cosmochim. Acta. 284 (2020) 107–119. https://doi.org/10.1016/j.gca.2020.06.021.

[34] N.E. Keon, C.H. Swartz, D.J. Brabander, C. Harvey, H.F. Hemond, Validation of an Arsenic Seqential Extraction Method for Evaluating Mobility in Sediments, Environ. Sci. Technol. 35 (2001) 2778–2784. https://doi.org/10.1021/es001511o.

[35] S.W. Poulton, D.E. Canfield, Development of a sequential extraction procedure for iron: Implications for iron partitioning in continentally derived particulates, Chem. Geol. 214 (2005) 209–221. https://doi.org/10.1016/j.chemgeo.2004.09.003.

[36] M. V. Schaefer, X. Guo, Y. Gan, S.G. Benner, A.M. Griffin, C.A. Gorski, Y. Wang, S. Fendorf, Redox controls on arsenic enrichment and release from aquifer sediments in central Yangtze River Basin, Geochim. Cosmochim. Acta. 204 (2017) 104–119. https://doi.org/10.1016/j.gca.2017.01.035.

[37] E. Viollier, P.W. Inglett, K. Hunter, A.N. Roychoudhury, P. Van Cappellen, The Ferrozine Method Revisited: Fe (II)/Fe (III) Determination in Natural Waters, Appl. Geochemistry. 15 (2000) 785–790. https://doi.org/10.1016/S0883-2927(99)00097-9.

[38] D.G. Rancourt, J.Y. Ping, Voigt-based methods for arbitrary-shape static hyperfine parameter distributions in Mössbauer spectroscopy, Nucl. Inst. Methods Phys. Res. B. 58 (1991) 85–97. https://doi.org/10.1016/0168-583X(91)95681-3.

[39] B. Ravel, M. Newville, ATHENA, ARTEMIS, HEPHAESTUS: Data analysis for X-ray absorption spectroscopy using IFEFFIT, J. Synchrotron Radiat. 12 (2005) 537–541. https://doi.org/10.1107/S0909049505012719.

[40] H. Guo, Y. Jia, R.B. Wanty, Y. Jiang, W. Zhao, W. Xiu, J. Shen, Y. Li, Y. Cao, Y. Wu, D. Zhang, C. Wei, Y. Zhang, W. Cao, A. Foster, Contrasting distributions of groundwater arsenic and uranium in the western Hetao basin, Inner Mongolia: Implication for origins and fate controls, Sci. Total Environ. 541 (2016) 1172–1190. https://doi.org/10.1016/j.scitotenv.2015.10.018.

[41] H.Y. Wang, H.M. Guo, W. Xiu, J. Bauer, G.X. Sun, X.H. Tang, S. Norra, Indications that weathering of evaporite minerals affects groundwater salinity and As mobilization in aquifers of the northwestern Hetao Basin, China, Appl. Geochemistry. 109 (2019) 104416. https://doi.org/10.1016/j.apgeochem.2019.104416.

[42] R.C. Davey, J.H.S. Macquaker, M. Siddiqi, C.D. Curtis, J.M. Williams, Applications of Mössbauer spectroscopy in the geochemistry of sedimentary rocks, Hyperfine Interact. 41 (1988) 771–774. https://doi.org/10.1007/BF02400504.

[43] L.K. Thomasarrigo, C. Mikutta, J. Byrne, K. Barmettler, A. Kappler, R. Kretzschmar, Iron and arsenic speciation and distribution in organic flocs from streambeds of an arsenic-enriched peatland, Environ. Sci. Technol. 48 (2014) 13218–13228. https://doi.org/10.1021/es503550g.

[44] C. Chen, R.K. Kukkadapu, O. Lazareva, D.L. Sparks, Solid-Phase Fe Speciation along the Vertical Redox Gradients in Floodplains using XAS and Mössbauer Spectroscopies, Environ. Sci. Technol. 51 (2017) 7903–7912. https://doi.org/10.1021/acs.est.7b00700.

[45] E. Eiche, U. Kramar, Z. Berner, S. Norra, M. Berg, T. Neumann, Behaviour of As in sequential sediment extractions observed by muSy-XRF analysis, Geochim. Cosmochim. Acta Suppl. 73 (2009) A320.

[46] K. Wallmann, K. Hennies, I. König, W. Petersen, H.D. Knauth, New procedure for determining reactive Fe(III) and Fe(II) minerals in sediments, Limnol. Oceanogr. 38 (1993) 1803–1812. https://doi.org/10.4319/lo.1993.38.8.1803.

[47] P.A. O'Day, N. Rivera, R. Root, S.A. Carroll, X-ray absorption spectroscopic study of Fe reference compounds for the analysis of natural sediments, Am. Mineral. 89 (2004) 572–585. https://doi.org/10.2138/am-2004-0412.

[48] D.R. Lovley, F.H. Chapelle, J.C. Woodward, Use of Dissolved H2 Concentrations To Determine Distribution of Microbially Catalyzed Redox Reactions in Anoxic Groundwater, Environ. Sci. Technol. 28 (1994) 1205–1210. https://doi.org/10.1021/es00056a005.

[49] T. Borch, R. Kretzschmar, K. Campbell, Biogeochemical Redox Processes and Their Impact on Contaminant Dynamics Biogeochemical Redox Processes and their Impact on Contaminant Dynamics, Environ. Sci. Technol. (2009) 15–23. https://doi.org/10.1021/es9026248.

[50] D. Postma, F. Larsen, N.T. Thai, P.T.K. Trang, R. Jakobsen, P.Q. Nhan, T.V. Long, P.H. Viet, A.S. Murray, Groundwater arsenic concentrations in Vietnam controlled by sediment age, Nat. Geosci. 5 (2012) 656–661. https://doi.org/10.1038/ngeo1540.

[51] E.C. Gillispie, A.R. Matteson, O.W. Duckworth, R.B. Neumann, N. Phen, M.L. Polizzotto, Chemical variability of sediment and groundwater in a Pleistocene aquifer of Cambodia: Implications for arsenic pollution potential, Geochim. Cosmochim. Acta. 245 (2019) 441–458. https://doi.org/10.1016/j.gca.2018.11.008.

[52] P.H. Viet, A. Lightfoot, R. Kipfer, E. Eiche, A. Kontny, T. Neumann, M. Glodowska, M.

564 Patzner, A. Kappler, B. Rathi, O. Cirpka, B. Bostick, Spatial and temporal evolution of
565 groundwater arsenic contamination in the Red River delta, Vietnam: Interplay of
566 mobilisation and retardation processes, Sci. Total Environ. (2020) 137143.
567 https://doi.org/10.1016/j.scitotenv.2020.137143.

568 [53] A. Burnol, L. Charlet, Fe(II)-Fe(III)-bearing phases as a mineralogical control on the
569 heterogeneity of arsenic in southeast Asian groundwater, Environ. Sci. Technol. 44 (2010)
570 7541–7547. https://doi.org/10.1021/es100280h.

571 [54] D. Postma, S. Jessen, N.T.M. Hue, M.T. Duc, C.B. Koch, P.H. Viet, P.Q. Nhan, F. Larsen,
572 Mobilization of arsenic and iron from Red River floodplain sediments, Vietnam,
573 Geochim. Cosmochim. Acta. 74 (2010) 3367–3381.
574 https://doi.org/10.1016/j.gca.2010.03.024.

575 [55] J.W. Stuckey, M. V. Schaefer, S.G. Benner, S. Fendorf, Reactivity and speciation of
576 mineral-associated arsenic in seasonal and permanent wetlands of the Mekong Delta,
577 Geochim. Cosmochim. Acta. 171 (2015) 143–155.
578 https://doi.org/10.1016/j.gca.2015.09.002.

579 [56] H.U. Sø, D. Postma, V.H. Hoang, L. Vi Mai, T. Pham Thi Kim, V. Pham Hung, R.
580 Jakobsen, Arsenite adsorption controlled by the iron oxide content of Holocene Red River
581 aquifer sediment, Geochim. Cosmochim. Acta. 239 (2018) 61–73.
582 https://doi.org/10.1016/j.gca.2018.07.026.

583 [57] W. Stumm, B. Sulzberger, The cycling of iron in natural environments: Considerations
584 based on laboratory studies of heterogeneous redox processes, Geochim. Cosmochim.
585 Acta. 56 (1992) 3233–3257. https://doi.org/10.1016/0016-7037(92)90301-X.

[58] N. Van Groeningen, L.K. ThomasArrigo, J.M. Byrne, A. Kappler, I. Christl, R. Kretzschmar, Interactions of ferrous iron with clay mineral surfaces during sorption and subsequent oxidation, Environ. Sci. Process. Impacts. 22 (2020) 1355–1367. https://doi.org/10.1039/d0em00063a.

[59] C. Schultz, T. Grundl, pH Dependence of ferrous sorption onto two smectite clays, Chemosphere. 57 (2004) 1301–1306. https://doi.org/10.1016/j.chemosphere.2004.09.023.

[60] H. Guo, D. Zhang, P. Ni, Y. Cao, F. Li, Y. Jia, H. Li, L. Wan, G. Wang, On the scalability of hydrogeochemical factors controlling arsenic mobility in three major inland basins of P.R. China, Appl. Geochemistry. 77 (2017) 15–23. https://doi.org/10.1016/j.apgeochem.2016.05.006.

[61] K. Pi, Y. Wang, D. Postma, T. Ma, C. Su, X. Xie, Vertical variability of arsenic concentrations under the control of iron-sulfur-arsenic interactions in reducing aquifer systems, J. Hydrol. 561 (2018) 200–210. https://doi.org/10.1016/j.jhydrol.2018.03.049.

[62] H.U. Sø, D. Postma, M.L. Vi, T.K.T. Pham, J. Kazmierczak, V.N. Dao, K. Pi, C.B. Koch, H.V. Pham, R. Jakobsen, Arsenic in Holocene aquifers of the Red River floodplain, Vietnam: Effects of sediment-water interactions, sediment burial age and groundwater residence time, Geochim. Cosmochim. Acta. 225 (2018) 192–209. https://doi.org/10.1016/j.gca.2018.01.010.

[63] H. Hagiwara, J. Akai, K. Terasaki, T. Yoshimura, H. Luo, Black colored sandy sediments caused by bacterial action, and the mechanism for arsenic enrichment of groundwater in Inner Mongolia, Appl. Geochemistry. 26 (2011) 380–393. https://doi.org/10.1016/j.apgeochem.2010.12.011.

[64] M.L. Farquhar, J.M. Charnock, F.R. Livens, D.J. Vaughan, Mechanisms of arsenic uptake from aqueous solution by interaction with goethite, lepidocrocite, mackinawite, and pyrite: An X-ray absorption spectroscopy study, Environ. Sci. Technol. 36 (2002) 1757–1762. https://doi.org/10.1021/es010216g.

[65] P.A.O. Day, D. Vlassopoulos, R. Root, N. Rivera, The influence of sulfur and iron on dissolved arsenic concentrations in the shallow subsurface under changing redox conditions, Proceeding Natl. Acad. Sci. (2004). https://doi.org/10.1073/pnas.0402775101.

[66] B. Planer-Friedrich, J. Schaller, F. Wismeth, J. Mehlhorn, S.J. Hug, Monothioarsenate Occurrence in Bangladesh Groundwater and Its Removal by Ferrous and Zero-Valent Iron Technologies, Environ. Sci. Technol. 52 (2018) 5931–5939. https://doi.org/10.1021/acs.est.8b00948.

[67] S. Stauder, B. Raue, F. Sacher, Thioarsenates in sulfidic waters, Environ. Sci. Technol. 39 (2005) 5933–5939. https://doi.org/10.1021/es048034k.

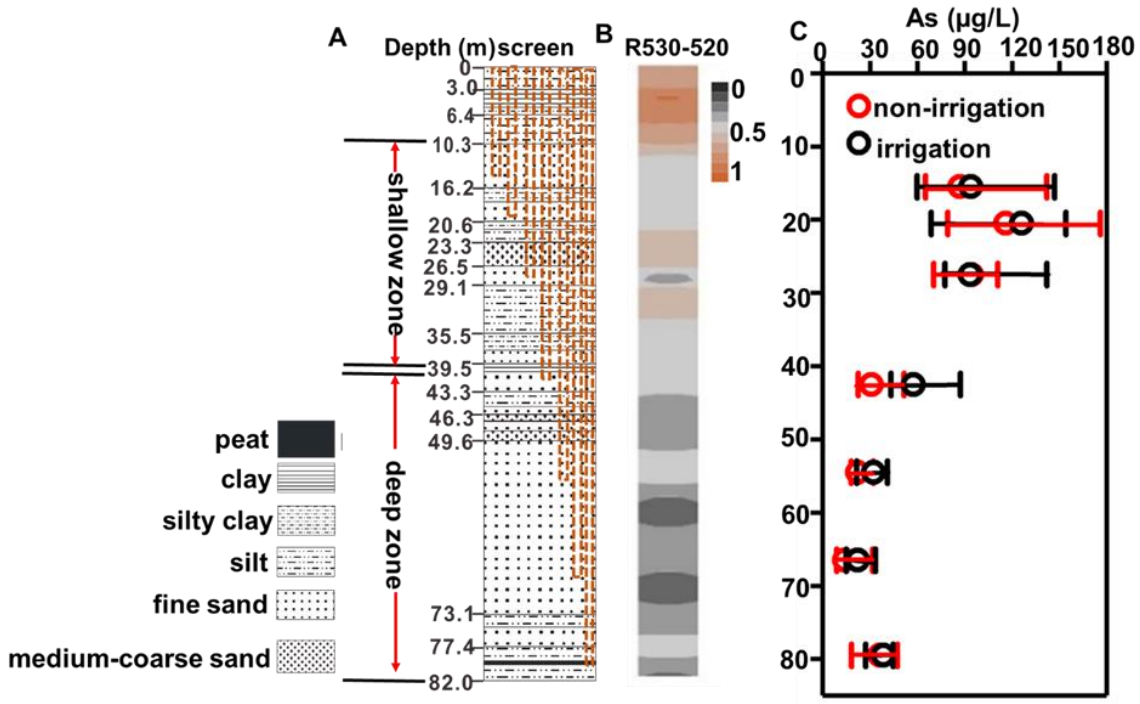

623

624 **Fig. 1** Plots of sediments lithologies (A), depths of screens, difference in reflectance at 530 nm
625 and 520 nm for the sediments (B), and monitoring data for groundwater As concentration (C).
626 Difference in reflectance between 530 nm and 520 nm indicated the color of collected sediments
627 [7]. The center circle showed the median value of As concentration in each screen, while the edge
628 of bars showed the min and max values. The reflectance data and groundwater As monitoring data
629 are previously shown in Zhang et al. [32].

630

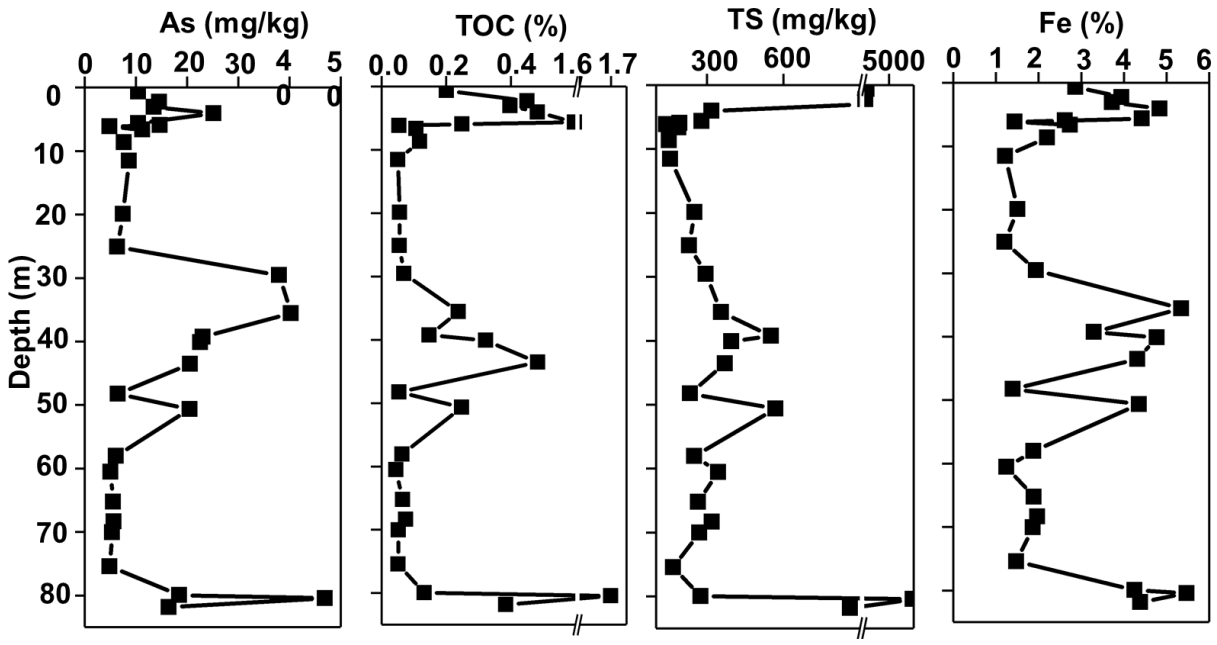

631

632 **Fig. 2** Depth profile of As, total organic carbon (TOC), total sulfur (TS) and Fe content in the

633 sediments. The data is referred to Wang et al., [33].

634

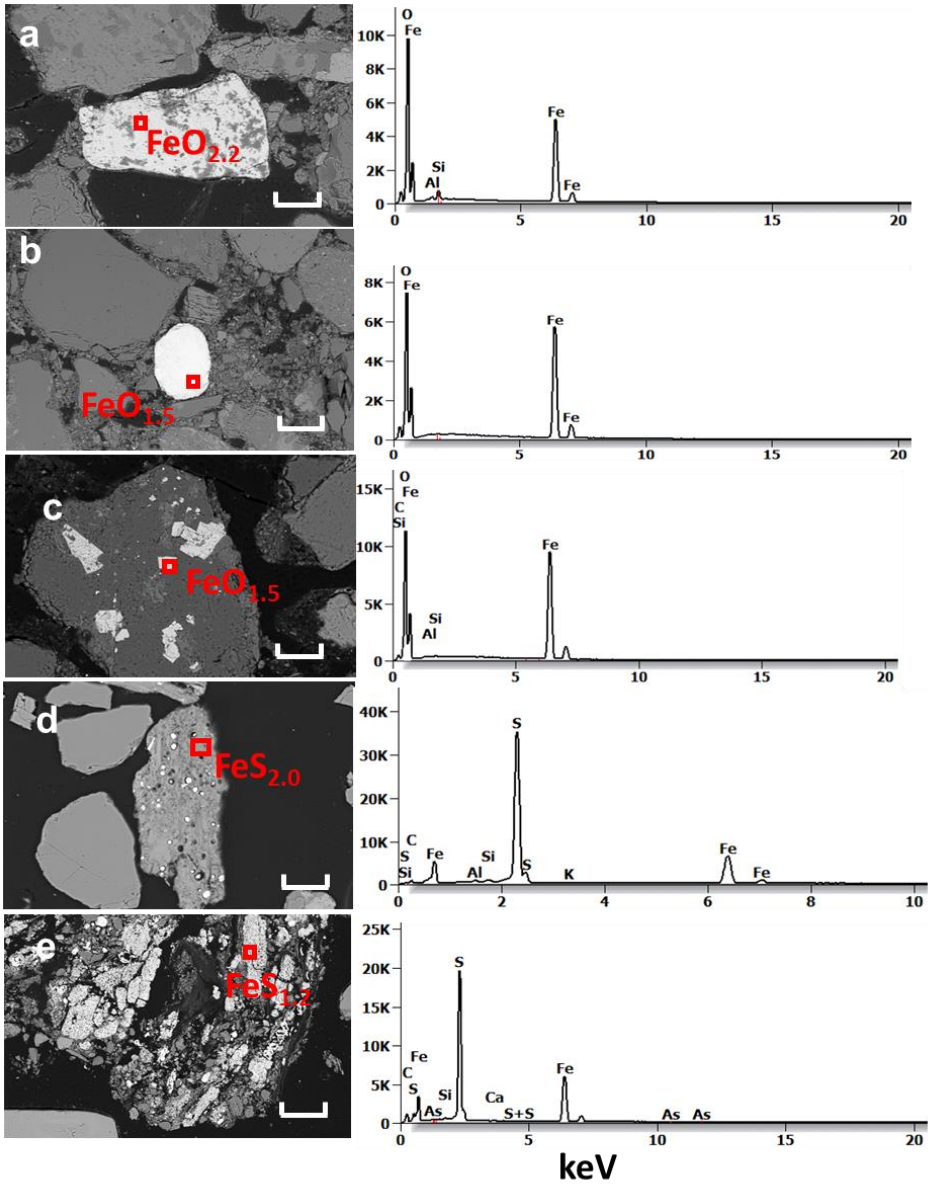

635

636 **Fig. 3** Iron oxides/Fe sulfides characterized by SEM-EDX. The Fe oxides shown in primary
637 sediments (a, b, c), Fe sulfides shown at depth of 29 m and 80 m (d, e). The EDX spectra
638 corresponded to chemical compositions of minerals marked with the red square in the SEM images
639 and the EDX data was shown in **Table S2**. The scale bar in each image represents 40 μm.

640

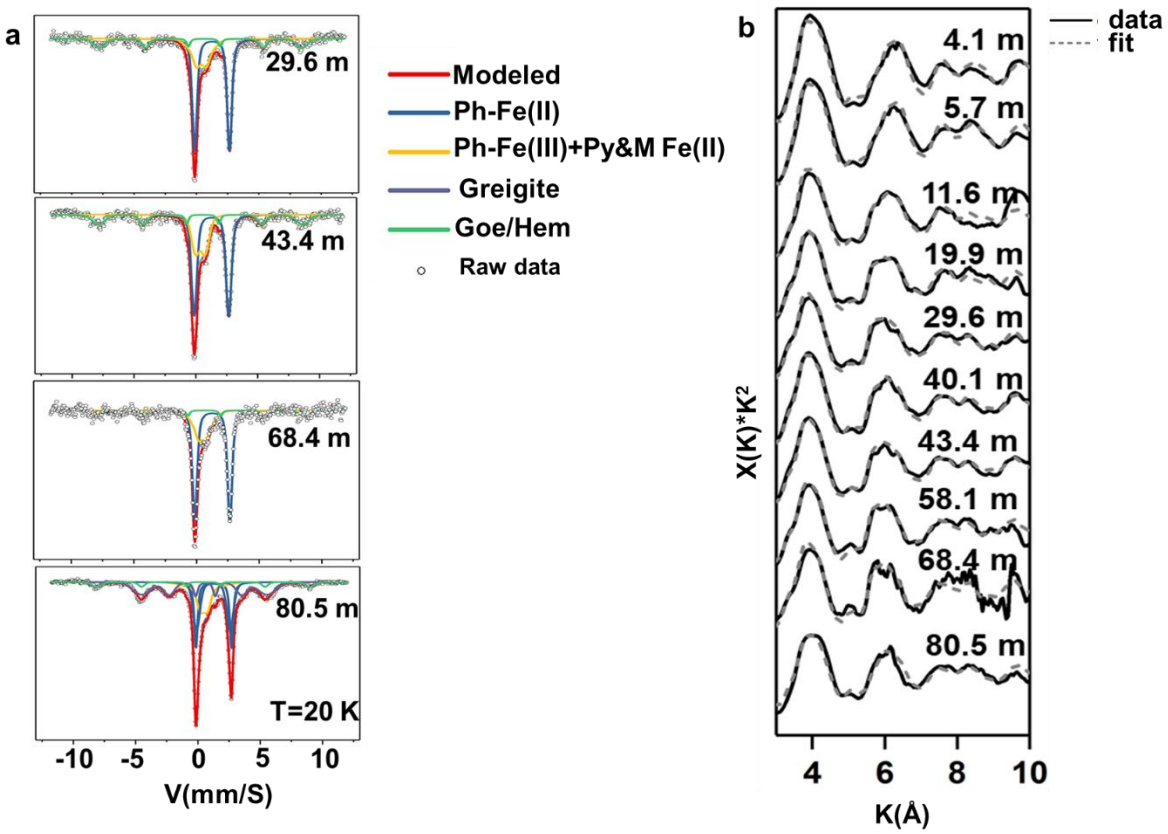

641

642 **Fig. 4** The ^{57}Fe Mössbauer spectra was collected at 20 K for sediments (a), ph: phyllosilicates; py:
643 pyrite; M: mackinawite; Goe: goethite; Hem: hematite. Liner combination fitting (LCF) results of
644 Fe K-edge EXAFS spectra (b), black lines represented experimental data for samples and model
645 compound spectra used for fitting, and gray dashed lines represented LCF. Fe K-edge EXAFS
646 reference spectra are shown in **Fig. S1**. Mössbauer and Fe K-edge EXAFS spectra for sediments
647 from depth of 80.5 m are referred from Wang et al., [33].

648

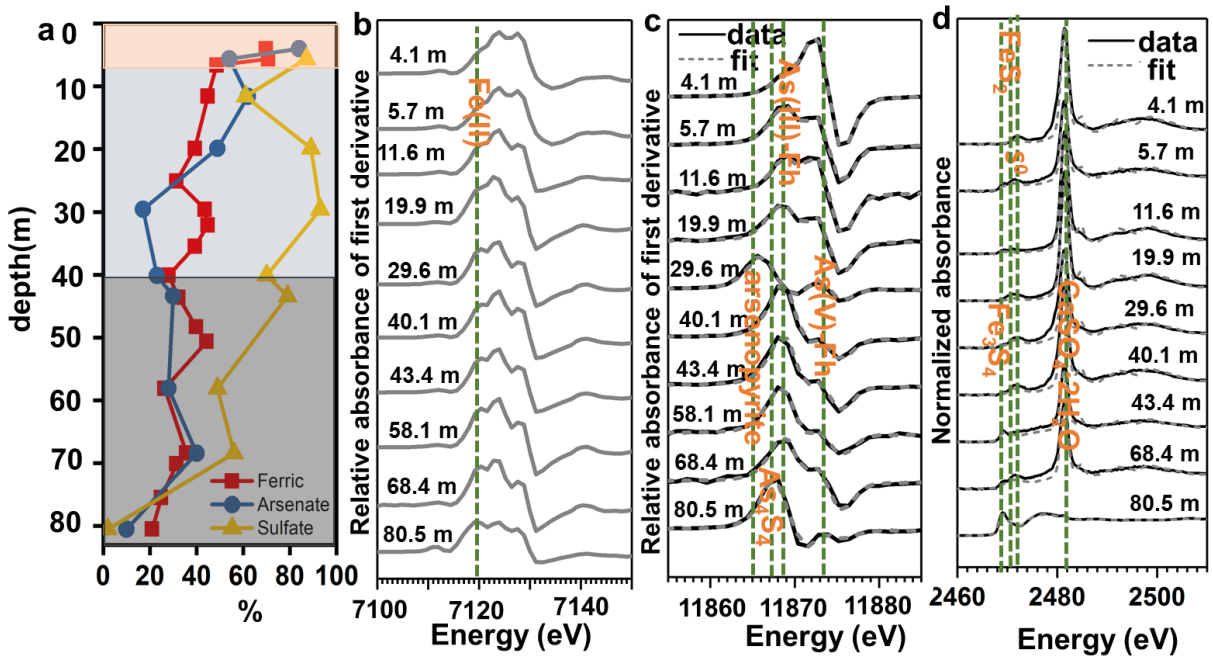

649

650 **Fig. 5** Depth patterns of ferric fraction from 2 M HCl extraction, arsenate fraction (mol %)
651 resulting from As K-edge derivative XANES fitting, and sulfate fraction (mol %) from S K-edge
652 XANES fitting (a). 1st derivative of Fe K-edge XANES data (b), 1st derivative of As K-edge
653 XANES data and fits (c), sulfur K-edge XANES data and fits (d), vertical dashed lines
654 corresponded to peak positions of respective speciation/reference spectra. The reference spectra
655 are shown in **Fig. S1**. The As K-edge derivative XANES data and sulfur K-edge XANES data for
656 sample from depth of 80.5 are cited from previous study [33].

657

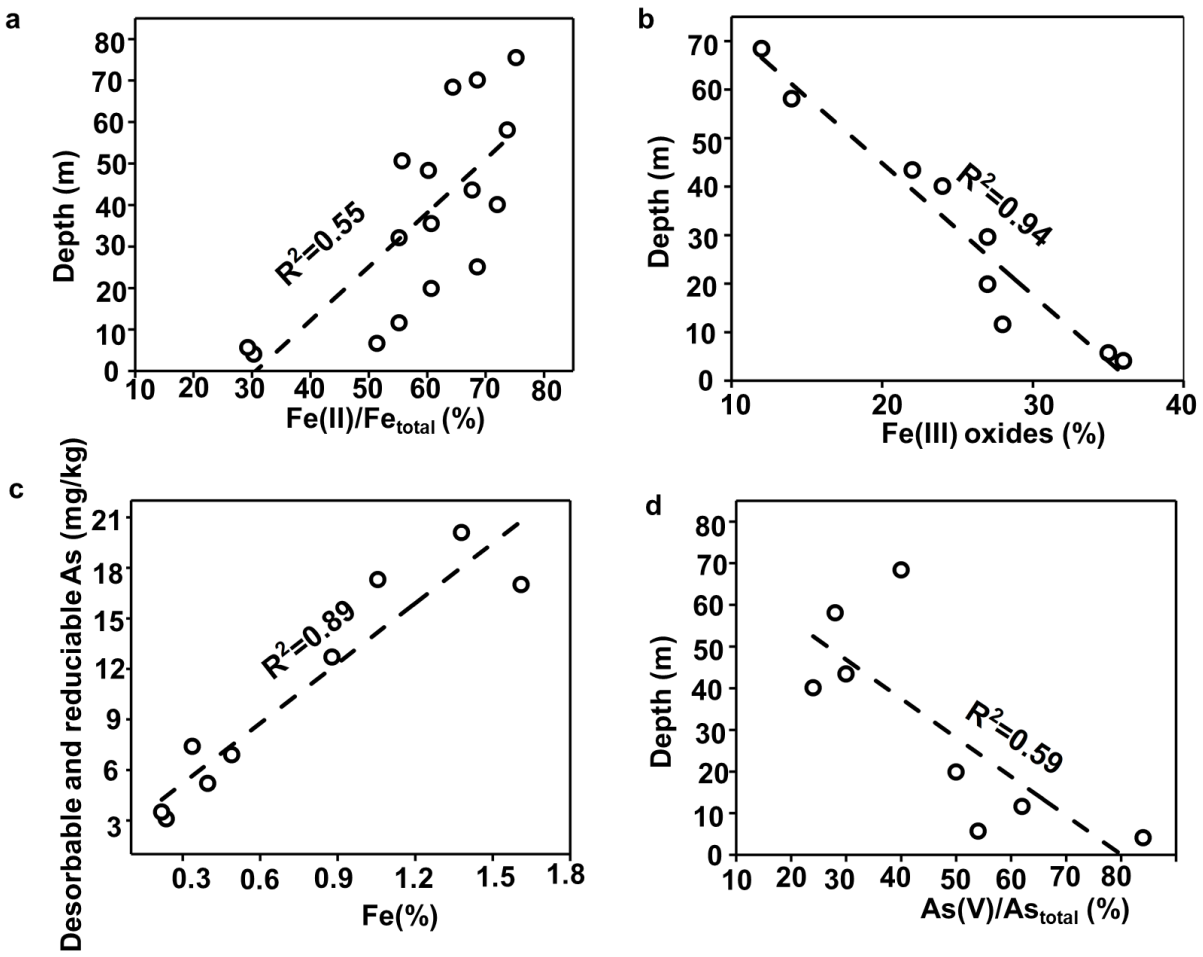

Fig. 6 Bivariate correlation between sample depth and ratio of Fe(II)/Fe from 2 M HCl extractions (a), bivariate correlation between sample depth and abundance of Fe(III) oxides (hematite and goethite) characterized by LCF in the Fe K-edge EXAFS range, correlation between sum of desorb-able(ligand-displaceable) and reducible As content and sum of goethite and hematite (calculated as Fe content) characterized by Fe K-edge EXAFS fitting (c), correlation between depth and arsenate fraction resulting from As K-edge derivative XANES LCF (d).

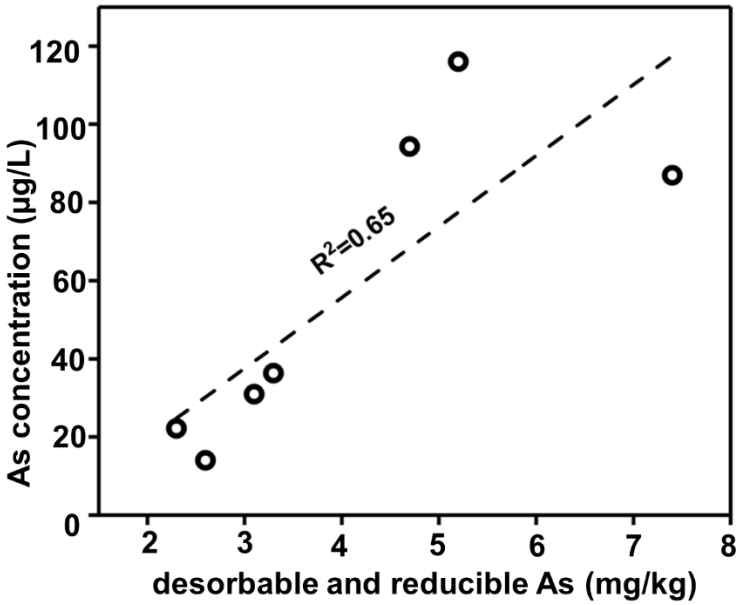

666

667 **Fig. 7** Bivariate relationships between desorbable and reducible As in sediments and As

668 concentration in the groundwater.

669

Table 1 Summary of S, Fe and As K-edge XANES or EXAFS LCF fitting results

Depth (m)	Mineralogical composition (% mol Fe)					
	EXAFS					
	illite	**biotite /chlorite**	**hematite**	**goethite**	**Fe sulfide**	**R^2**
4.1	53 (0.4)	10 (2.0)	12 (1.9)	24 (5.8)	-	0.0521
5.7	56 (4.4)	10 (2.2)	10 (2.0)	25 (5.7)	-	0.0471
11.6	30 (6.2)	34 (4.7)	10 (2.9)	18 (10.3)	8 (4.9)	0.1219
19.9	24 (4.8)	41 (3.6)	11 (2.3)	16 (4.2)	10 (3.8)	0.0809
29.6	18 (3.2)	55 (4.7)	7 (1.5)	20 (2.9)	-	0.0467
40.1	31 (4.8)	42 (1.3)	9 (1.0)	15 (2.3)	-	0.0240
43.4	26 (2.9)	43 (2.2)	5 (1.4)	17 (4.5)	-	0.0305
58.1	23 (7.9)	46 (3.3)	-	14 (3.9)	15 (3.5)	0.0743
68.4	31 (7.2)	49 (13)	-	12 (6.3)	5 (5.7)	0.1711
80.5	37 (4.4)	19 (2.4)	-	-	39 (3.3)	0.0911

Depth (m)	Mineralogical composition (% mol As)					Mineralogical composition (% mol S)			
	XANES first-derivative					**XANES**			
	realgar	**arsenopyrite**	**As (III)-Fh**	**As (V)-Fh**	**R^2**	**sulfates**	**sulfides**	**S_0**	**R**
4.1	-	-	16 (2.5)	84 (0)	0	--	--	--	--
5.7	-	-	46 (0.6)	54 (0.6)	0.0057	87 (1.6)	-	13 (1.6)	0.0575
11.6	-	-	38 (4.5)	62 (1.0)	0.0170	61 (7.7)	23 (5.4)	16 (5.4)	0.0416
19.9	7 (0.9)	-	44 (1.4)	49 (0.6)	0.0074	89 (0.8)	11 (1.3)	-	0.0160
29.6	-	62 (3.7)	21 (0.7)	17 (0.5)	0.0102	93 (1.8)	7.3 (0.9)	-	0.0185
40.1	-	-	76 (0.6)	24 (0.8)	0.0072	70 (1.5)	6.5 (8.3)	23 (8)	0.0710
43.4	-	-	70 (3.4)	30 (1.0)	0.0213	79 (2.0)	-	21 (1.4)	0.0534
58.1	9 (1.5)	-	63 (1.3)	28 (0.8)	0.0123	49 (0.8)	51 (7.6)	-	0.0368
68.4	-	-	60 (0.9)	40 (0.9)	0.0195	56 (9.4)	23 (7)	21 (7)	0.0680
80.5	40 (5.0)		50 (1.8)	10 (1.1)	0.0197	2 (0.7)	92 (0.7)	6 (0.6)	0.0058

--: samples not measured, -: not detected or abundance lower than 5%. Values within brackets indicate standard deviation, Fe sulfide exists as FeS, except it shows as greigite in the depth of 80.4 m. Results for samples from depth of 80.5m are referred to Wang et al., [33].

675 **Table 2** Summary of extracted As contents (mg/kg) from each sequential step.

Depth (m)	S1	S2	S3	S4	S3+S4	S5	As extracted	Total As
4.1	7.0	0.6	6.4	3.6	10	2.4	20.0	22
5.7	10.8	1.2	6.6	2.7	9.3	1.0	22.3	15
6.7	2.5	0.3	2.2	5.0	7.2	1.1	11.1	11
11.6	2.8	0.4	1.8	2.8	4.6	0.4	8.2	9
19.9	2.2	0.3	1.4	1.6	3	0.6	6.1	8
25.1	2.2	0.3	1.1	1.4	2.5	0.4	5.4	6
29.6	3.0	0.5	1.4	2.5	3.9	0.8	8.3	9
35.6	9.9	1.1	3.0	5.2	8.2	1.4	20.6	40
40.1	11.0	1.1	3.1	3.2	6.3	1.4	19.8	23
43.6	8.1	0.8	3.0	1.6	4.6	0.9	14.4	21
48.3	1.6	0.3	1.0	1.5	2.5	0.7	5.1	7
50.5	4.8	1.2	4.4	6.0	10.4	0.9	17.3	21
58.1	1.5	0.4	0.8	0.8	1.6	0.6	4.1	6.1
68.4	1.8	0.3	0.9	0.8	1.7	0.5	4.3	5.7
70.1	1.9	0.3	0.8	1.2	2	0.5	4.7	5.4
75.5	1.0	0.3	1.4	0.9	2.3	0.5	4.1	4.9
80.4	31.9	12.9	3.2	2.4	5.6	3.9	54.3	46

676

677

678

679